J Mater Sci (2006) 41:6266–6273
DOI 10.1007/s10853-006-0512-y

Fatigue crack propagation in microcapsule-toughened epoxy

E. N. Brown · S. R. White · N. R. Sottos

Received: 4 May 2004 / Accepted: 1 September 2005 / Published online: 12 August 2006

Abstract The addition of liquid-filled urea-formaldehyde (UF) microcapsules to an epoxy matrix leads to significant reduction in fatigue crack growth rate and corresponding increase in fatigue life. Mode-I fatigue crack propagation is measured using a tapered double-cantilever beam (TDCB) specimen for a range of microcapsule concentrations and sizes: 0, 5, 10, and 20% by weight and 50, 180, and 460 μm diameter. Cyclic crack growth in both the neat epoxy and epoxy filled with microcapsules obeys the Paris power law. Above a transition value of the applied stress intensity factor ΔK_T, which corresponds to loading conditions where the size of the plastic zone approaches the size of the embedded microcapsules, the Paris law exponent decreases with increasing content of microcapsules, ranging from 9.7 for neat epoxy to approximately 4.5 for concentrations above 10 wt% microcapsules. Improved resistance to fatigue crack propagation, indicated by both the decreased crack growth rates and increased cyclic stress intensity for the onset of unstable fatigue-crack growth, is attributed to toughening mechanisms induced by the embedded microcapsules as well as crack shielding due to the release of fluid as the capsules are ruptured. In addition to increasing the inherent fatigue life of epoxy, embedded microcapsules filled with an appropriate healing agent provide a potential mechanism for self-healing of fatigue damage.

E. N. Brown (✉) · N. R. Sottos
Department of Theoretical and Applied Mechanics and the Beckman Institute for Advanced Science and Technology, University of Illinois at Urbana-Champaign, 216 Talbot Laboratory, 104 S. Wright St., Urbana, IL 61801, USA
e-mail: en_brown@lanl.gov

N. R. Sottos
e-mail: n-sottos@uiuc.edu

Present Address:
E. N. Brown
Materials Science and Technology Division, MS G-755, Los Alamos National Laboratory, Los Alamos, NM 87545, USA

S. R. White
Department of Aerospace Engineering and the Beckman Institute for Advanced Science and Technology, University of Illinois at Urbana-Champaign, 306 Talbot Laboratory, 104 S. Wright St., Urbana, IL 61801, USA
e-mail: swhite@uiuc.edu

Introduction

Highly crosslinked epoxy resins have low strain-to-failure and exhibit poor resistance to crack propagation. Fatigue loading is particularly problematic, causing small cracks to initiate and grow rapidly. These cracks often lead to catastrophic failure. An extensive body of work exists for the general area of fatigue of polymers [1–3], which focuses on understanding the mechanisms of fatigue and predicting the rates of fatigue-crack growth.

Fatigue crack propagation studies are performed with the cyclic-crack-tip stress state varying over a range defined by $\Delta K_I \equiv (K_{max} - K_{min})$. Dependence of the fatigue-crack-growth rate da/dN on the applied range of stress intensity factors ΔK_I is generally described by the empirical Paris law equation [4]

$$\frac{da}{dN} = C_0 \Delta K_I^n, \tag{1}$$

where C_0 and n are material constants that depend on the ratio of applied stress intensity $R \equiv K_{min}/K_{max}$, the loading frequency f, and the testing environment. The typical crack growth behavior described by Eq. (1) yields a linear log–log plot that is bounded by a threshold stress intensity range ΔK_{th} below which a crack ceases to propagate, and the critical stress intensity K_{IC} above which crack growth in unstable.

Several researchers [5–7] have successfully measured fatigue-crack propagation in epoxy resins and obtained values of the Paris law exponent n on the order of 10. Incorporation of either a rubbery second phase [8–11] or solid particles [7, 12, 13] significantly improves the resistance to fatigue-crack propagation. Several of these studies [5, 8, 9, 11, 13, 14] suggest that improvements in the resistance to fatigue crack propagation behavior are also associated with increased toughness in monotonic fracture [1, 2, 14, 15].

Previously, we investigated the effect of embedded urea-formaldehyde (UF) microcapsules on the monotonic fracture properties of a self-healing epoxy [15]. In addition to providing an efficient mechanism for self-healing [16–18], the presence of liquid-filled microcapsules increased the virgin monotonic–fracture toughness of epoxy by up to 127% [15, 17]. The increased toughening was correlated with a change in the fracture plane morphology from mirror-like to hackle markings with subsurface microcracking. The inherent fracture toughness as well as the healing efficiency both depended strongly on the size and concentration of microcapsules. In the current work, we extend this investigation to examine the influence of microcapsules on the fatigue crack propagation behavior of epoxy, with the effects of self-healing precluded. Consistent with the monotonic fracture studies, the addition of microcapsules to an epoxy matrix significantly increased the resistance to crack growth under dynamic loading conditions.

Experimental procedure

Materials and sample preparation

Urea-formaldehyde microcapsules containing dicyclopentadiene (DCPD) monomer were manufactured with average diameters of 50, 180, and 460 μm using the emulsion in situ polymerization microencapsulation method outlined by Brown et al. [19]. Shell wall thickness was 190 ± 30 nm for all batches. Tapered double-cantilever beam specimens were cast from EPON® 828 epoxy resin (DGEBA) and 12 pph Ancamine® DETA (diethylenetriamine) curing agent with a prescribed concentration of microcapsules mixed into the resin. The epoxy mixture was degassed, poured into a closed silicone rubber mold and cured for 24 h at room temperature, followed by 24 h at 30° C. Relevant physical and mechanical properties of the microcapsules and neat epoxy are listed in Table 1. The tensile modulus and mode I critical stress intensity factor, K_{IC}, of the microcapsule toughened epoxy were measured as a function of capsule concentration by Brown et al. [15, 20] and Rzeszutko et al. [21] and summarized in Table 2.

Mechanical testing

The fatigue-crack propagation behavior of the microcapsule-modified epoxy was investigated using the tapered double-cantilever beam (TDCB) specimen shown in Fig. 1. Side grooves ensured controlled crack growth along the centerline of the brittle specimen. The premise of the TDCB geometry, developed by Mostovoy et al. [22], was to provide a crack-length-independent relationship between applied stress intensity factor K_I and load P,

$$K_I = \alpha P, \tag{2}$$

which only required knowledge of the coefficient α. While no single TDCB geometry has been adopted as a standard, the literature contains numerous TDCB designs, most of which attempt to optimize the constant K region of the sample (see for examples [23–26]). Recently Mostovoy [27] introduced a new TDCB geometry and showed that for crack lengths of a/W (i.e. the crack length normalized by the length of the specimen) between 0.25 and 0.50 the error in this new sample design is 3%, compared to 15% for the original specimen [22]. However, more accurate TDCB designs are available in the literature and we adopted the geometry developed for fatigue crack growth experiments by Beres et al. [26]. Beres presented a comprehensive 3D FEM study to determine the divergence in

Table 1 Properties of the constituent materials [15]

Properties	Epoxy	Urea-formaldehyde microcapsules
Density (kg/m^3)	1160	~1000
Diameter (μm)	–	50 ± 20 180 ± 40 460 ± 80
Wall thickness (nm)	–	190±30
K_{IC} (MPa m$^{1/2}$)	0.55 ± 0.04	–
Young's modulus (GPa)	3.4 ± 0.1	–
Ultimate stress (MPa)	39 ± 4	–

Table 2 Mechanical properties of neat epoxy and epoxy with embedded microcapsules [15]

Microcapsule concentration (wt%)	Diameter, d (μm)	Young's modulus, E (GPa)	Critical stress intensity factor, K_{IC} (MPa $m^{1/2}$)	Critical strain energy release rate, G_C (J/m^2)
0	–	3.4 ± 0.1	0.55 ± 0.04	88 ± 14
5	50 ± 20	3.2 ± 0.1	1.1 ± 0.1	350 ± 70
10	50 ± 20	–	1.2 ± 0.2	–
20	50 ± 20	–	1.1 ± 0.1	–
5	180 ± 40	3.2 ± 0.1	0.78 ± 0.16	190 ± 90
10	180 ± 40	2.8 ± 0.1	1.2 ± 0.2	430 ± 170
20	180 ± 40	2.7 ± 0.1	1.0 ± 0.2	400 ± 130
10	460 ± 80	–	0.92 ± 0.07	–
20	460 ± 80	–	1.2 ± 0.1	–

K with increasing crack length and included the effect of varying side grooves. For crack lengths of a/W between 0.23 and 0.48 Beres's geometry has an error of less than 0.5% [26] which is supported by our own FEA, quasistatic compliance measurements, and constant crack growth rate fatigue experiments (methods and results presented in [15, 17, 20, 28]).

The sample in Fig. 1 is a modified version of the TDCB geometry developed and verified by Beres et al. [26], for which $\alpha = 11.2 \times 10^3\ m^{-3/2}$ was determined experimentally [17]. An extensive analysis of the TDCB geometry is provided in Brown [20]. Comparison of the current sample with Mostovoy's original reveals several improvements in the current design, most importantly the reduction of edge effects. A constant range of Mode-I stress intensity factor ΔK_I was achieved by applying a constant range of load ΔP, independent of crack length. The constant-K region of the TDCB specimen enables crack-growth-rate measurements over a range of cycles, rather than requiring use of the modified secant formulation commonly employed for changing ΔK_I of a compact tension specimen [14]. Moreover, the constant-K region is of great importance for observing the time-dependent effects of self-healing during growth of a fatigue-crack [20].

Fatigue crack propagation studies were performed using an Instron DynoMight 8841 low-load frame with 250 N load-cell. Samples were precracked with a razor blade while ensuring the precrack tip was centered in the groove and then pin loaded. A triangular frequency of 5 Hz was applied with a load ratio ($R = K_{min}/K_{max}$) of 0.1. Crack lengths were determined by optical measurements at finite times and by compliance-inferred measurements [29] acquired approximately every 256th cycle.

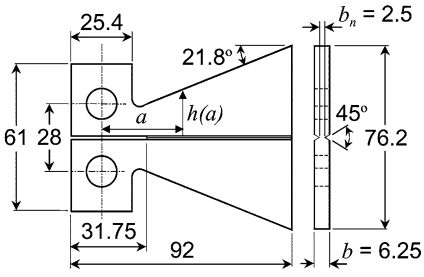

Fig. 1 Tapered-double-cantilever-beam geometry [17]. All dimensions in mm

The optically measured crack-tip position and specimen compliance are plotted against number of cycles in Fig. 2a. The linear relationship between optically measured crack length and specimen compliance (Fig. 2b) is used to calculate the crack-tip position at all times during the experiment (Fig. 2c). Crack-growth data are generated under constant ΔP (*i.e.* constant ΔK_I), with a complete set of loading conditions measured on a single specimen by incrementally increasing ΔP. Crack-growth rates are obtained from the number of cycles N required to grow a crack a distance Δa of approximately 1 mm for a given range of Mode-I stress intensity factor ΔK_I. Statistically equivalent values of crack-growth rate are obtain from using either the optically measured crack length prior to, $a_{i=0}^{opt}$, and following, $a_{i=S}^{opt}$, the application of N cycles at a give ΔK_I,

$$\left.\frac{da}{dN}\right|_{\Delta K} = \frac{\Delta a}{\Delta N} = \frac{a_{i=S}^{opt} - a_{i=0}^{opt}}{N_{i=s}}, \tag{3}$$

or from using a linear fit of the compliance-inferred measurements a_i^{comp},

$$\left.\frac{da}{dN}\right|_{\Delta K} = \frac{S\sum_{i=1}^{S} N_i a_i^{comp} - \sum_{i=1}^{S} N_i \sum_{i=1}^{S} a_i^{comp}}{S\sum_{i=1}^{S} N_i^2 - \left(\sum_{i=1}^{S} N_i\right)^2}, \tag{4}$$

where S is the total number of cycle samples acquired.

Fracture surface morphologies of the fatigue samples were examined with an environmental scanning electron microscope (Philips XL30 ESEM-FEG). After failure, specimens were mounted and sputtered

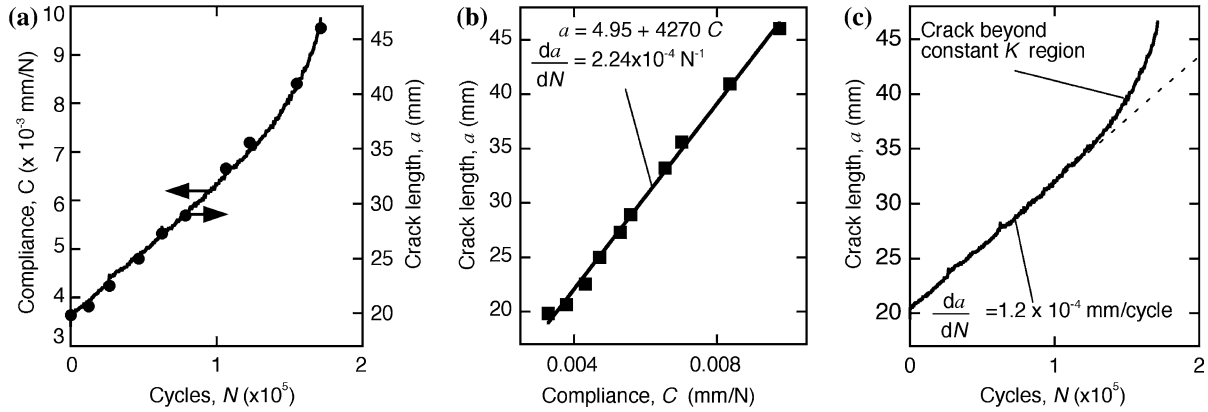

Fig. 2 Plots illustrating method to calculate the continuous crack-tip position from compliance data (–) and finite optical measurements (•) (**a**). (**b**) Linear fit of optically measured crack *vs.* specimen compliance. The squares (■) represent compliance values corresponding to the optical data and the line (–) represents the linear best fit. (**c**) Crack length calculated from measured compliance using the relationship obtained from (**b**) plotted *vs.* number of cycles. The specimen is neat epoxy; the test parameters are $f = 5$ Hz, $R = 0.1$, and $\Delta K_I = 0.472$ MPa $m^{1/2}$

with gold/palladium. Micrographs were obtained using 10 kV secondary electrons in high vacuum mode.

Results

The effect of embedded microcapsule concentration on fatigue crack growth is shown in Fig. 3 for 180 μm diameter microcapsules. The relationship between the crack growth rate d*a*/d*N* of epoxy and the applied range of Mode-I stress intensity factor ΔK_I clearly follows the Paris power law (Eq. 1). The measured Paris exponent is $n = 9.7$ for crack propagation in neat EPON® 828-Ancamine® DETA (no microcapsules). At applied stress intensity factors greater than $\Delta K \sim 0.35$ to 0.4 MPa $m^{1/2}$, a distinct transition in crack growth is observed for the microcapsule filled epoxy. Above a transition value ΔK_T, epoxy with microcapsules exhibits a higher resistance to fatigue crack growth than neat epoxy, accompanied by a reduction of the Paris law exponent n. At applied load levels below the transition point, the microcapsules have little influence on the crack growth rate.

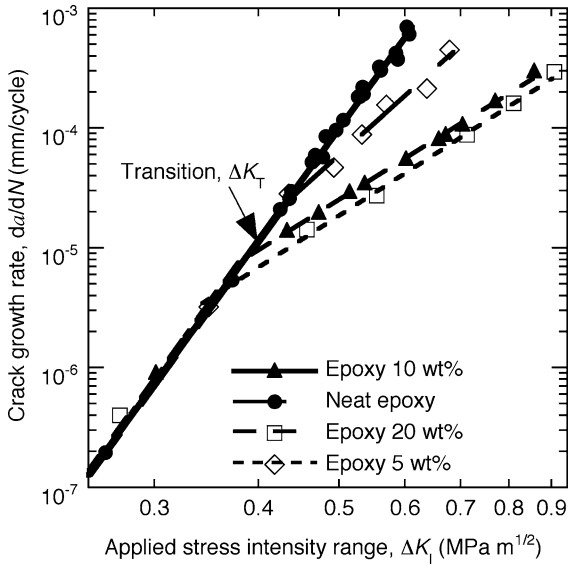

Fig. 3 Influence of microcapsule concentration on the fatigue crack growth behavior for 180 μm diameter microcapsules

Measured Paris law parameters for epoxy with embedded 50, 180, and 460 μm diameter microcapsules are summarized in Table 3. The Paris law exponent, n is plotted as a function of microcapsule concentration in Fig. 4. Above ΔK_T, the value of n decreases significantly with increasing microcapsule concentration, independent of capsule diameter. For concentrations greater than 10 wt% microcapsules, n has a steady-state value of approximately 4.5. Others have observed similar behavior for rubber-modified epoxies [14, 30].

The effect of the microcapsules on life extension is shown more clearly in Fig. 5 by comparison of crack length as a function of loading cycles for neat epoxy and epoxy with 20 wt% microcapsules above ΔK_T. The addition of microcapsules significantly increases fatigue life; for the loading condition of $\Delta K_I = 0.586$ MPa $m^{1/2}$ the fatigue life increases from 86×10^3 cycles for neat epoxy to 239×10^3 for the microcapsule filled system.

Examination of the fatigue-fracture surface for neat epoxy reveals a relatively featureless morphology (Fig. 6a–c). River markings [31] are observed on some fracture surfaces, but are only initiated at locations corresponding to the crack-tip position when ΔK_I is

Table 3 Constants of the Paris power law, ΔK_I^{max}, ΔK_T, and r_y

Microcapsule concentration (wt%)	Diameter (μm)	C_o (above ΔK_T)	n	ΔK_I^{max} (MPa $m^{1/2}$)	ΔK_T (MPa $m^{1/2}$)	r_y (μm)
0	–	8.2×10^{-2}	9.7	0.60	–	–
10	50 ± 20	1.5×10^{-3}	4.9	0.82	0.41	–
20	50 ± 20	1.6×10^{-3}	4.6	0.81	0.44	–
5	180 ± 40	4.2×10^{-3}	6.1	0.64	0.46	60 ± 30
10	180 ± 40	5.4×10^{-4}	4.4	0.82	0.40	70 ± 40
20	180 ± 40	3.8×10^{-4}	4.3	0.80	0.36	70 ± 30
10	460 ± 80	7.8×10^{-4}	4.4	0.64	0.40	–
20	460 ± 80	8.6×10^{-4}	4.7	0.82	0.39	–

incrementally increased (Fig. 6d–f). In contrast, the fatigue-fracture surface for epoxy with embedded microcapsules is characterized by substantial out-of-plane morphology at all length scales (Fig. 7). At the largest length scale, the microcapsules are ruptured at the fracture plane (similar to monotonic fracture), the fatigue-crack-growth path has significant deviation in and out of the plane, and the crack branches out of the plane at several locations (Fig. 7a). At smaller length scales the microcapsule walls have numerous secondary cracks (Fig. 7b, c) and the matrix has additional contortion and river markings at decreasing length scales (Fig. 7d, e).

Discussion

The addition of microcapsules significantly improves the fatigue response above a transition value of the applied stress intensity factor, ΔK_T. Similar improvements reported in the literature for rubber modified epoxies have been explained by effects of plastic zone size [11, 14] and increases of monotonic fracture toughness [5, 8, 9, 11, 13, 14]. Azimi et al. [12, 14] observed a transition point in the fatigue crack propagation behavior of DGEBA epoxies modified with CTBN and silicon rubber. Above a threshold value, the rubber-modified epoxy exhibited improved resistance to fatigue crack growth. Below the threshold, both neat epoxy and the rubber-modified epoxy had similar resistance. The transition was attributed to interactions between the rubber particles and the plastic zone present at the crack tip. Moreover, Azimi showed that the transition phenomenon was triggered when the size of the theoretical crack-tip plastic zone was of the order of the size of the filler.

Applying Azimi's hypothesis [12, 14] to microcapsule-toughened epoxy, the theoretical plastic zone size at a cyclically loaded crack tip is estimated based on Irwin's [32] formula for the size of a plastic zone,

$$r_y(\Delta K_T) = \frac{1}{2\pi}\left(\frac{\Delta K_T/(1-R)}{\sigma_{YS}}\right)^2, \quad (5)$$

where σ_{YS} is the yield stress of the epoxy with embedded microcapsules. In previous work, Irwin's formula accurately captured the plastic zone size in EPON® 828–Ancamine® DETA under monotonic

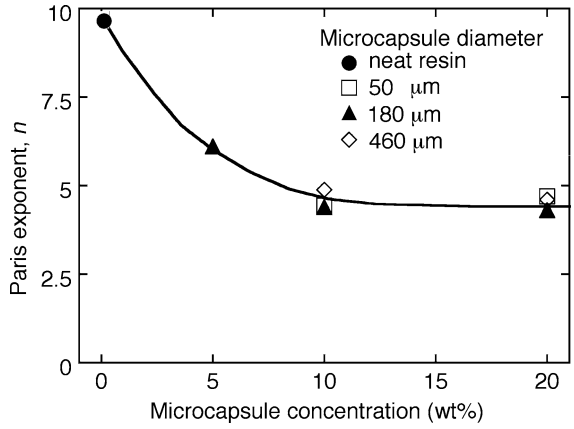

Fig. 4 Influence of microcapsule concentration on Paris law exponent, n

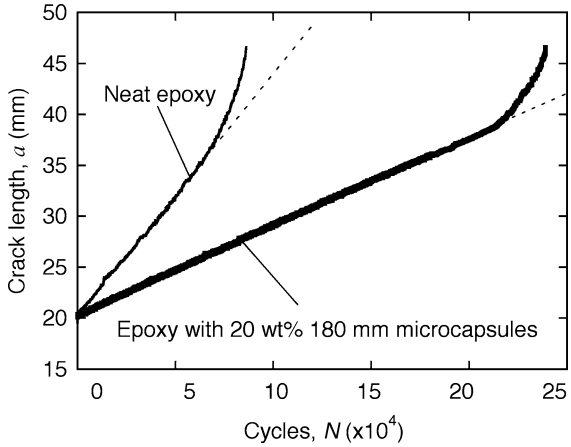

Fig. 5 Fatigue crack extension *vs.* number of cycles for neat epoxy and epoxy with 20 wt% 180 microcapsules. The test parameters are $f = 5$ Hz, $R = 0.1$, and $\Delta K_I = 0.586$ MPa $m^{1/2}$

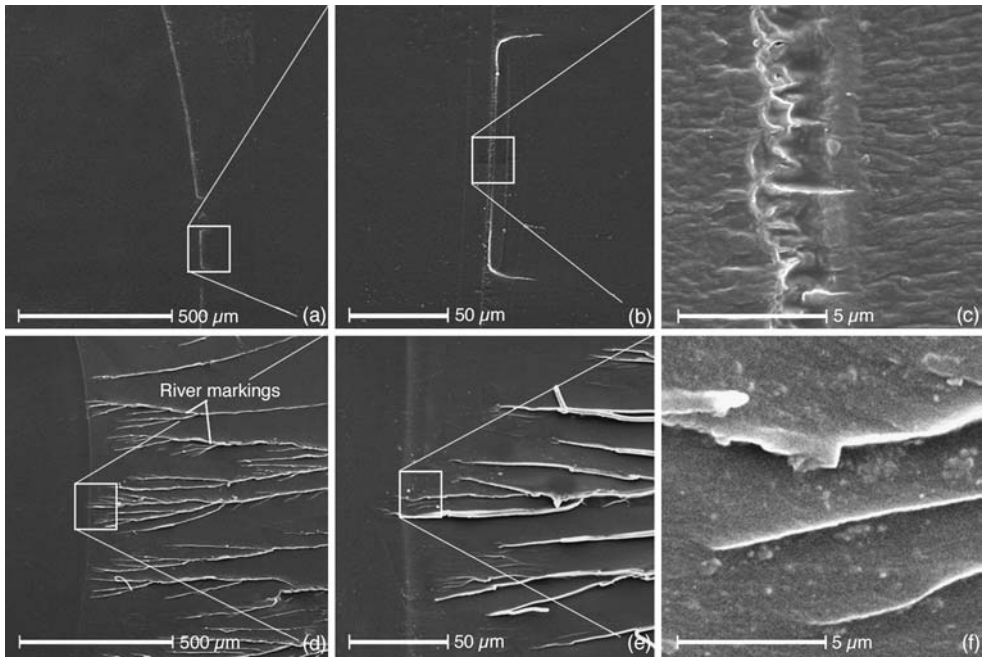

Fig. 6 Fatigue-fracture surfaces for neat epoxy. (**a**–**c**) The dominant surface morphology is featureless at different length scales and (**d**–**f**) has some local river markings. Note: The crack propagation is from left to right in all images

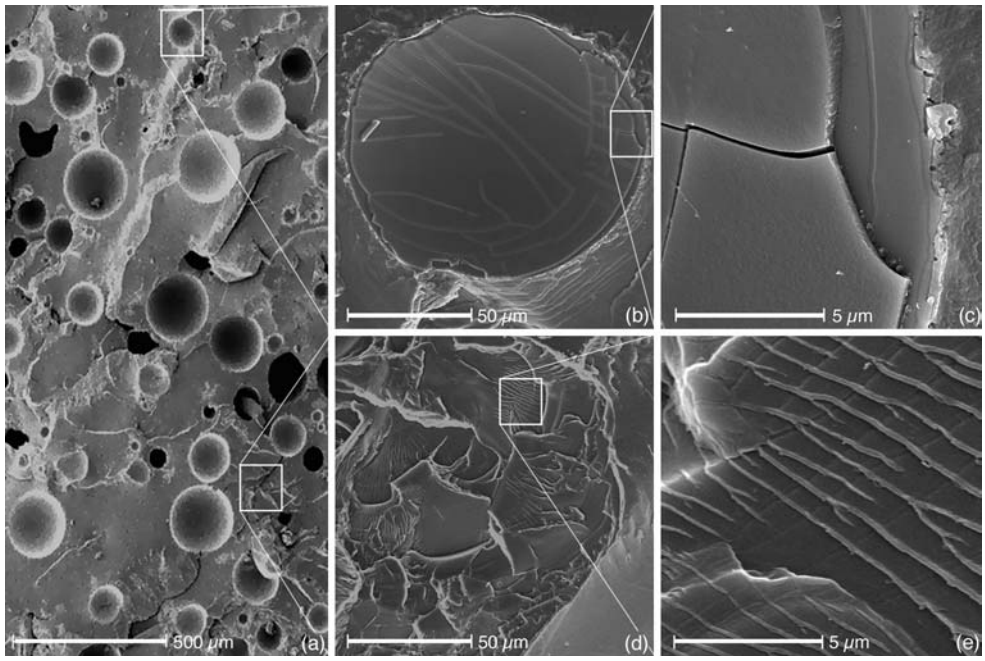

Fig. 7 Fatigue-fracture surfaces for epoxy with 20 wt% of 180 μm microcapsules. (**a**) At large length scales the fracture plane has a contorted crack-growth path and ruptured microcapsules. At smaller length scales (**b**, **c**) the microcapsules exhibit cracking and (**d**, **e**) the matrix has complex morphology. Note: The crack propagation is from left to right in all images

fracture conditions [15]. The plastic zone size estimated by Eq. (5) for 5, 10, and 20 wt% of 180 μm diameter microcapsules is c.a. 70 μm (assuming σ_{YS} = 20 MPa [15]). The calculated plastic zone size at the transition point for samples with 180 μm is within an order of magnitude of the microcapsule diameter consistent with Azimi's findings for 2–3 μm diameter rubber particles. When ΔK_I is less than ΔK_T, the plastic zone is smaller than the embedded microcapsules. In this regime the plastic zone is unaffected by the microcapsules—other than the presence of discontinuities along the crack front—resulting in little or no toughening and a fatigue response similar to that of the neat epoxy. When ΔK_I is greater than ΔK_T, the plastic zone is sufficiently large to encompass the majority of microcapsules in its path, activating toughening mechanisms similar to those observed for monotonic fracture.

The onset of fatigue crack growth instability is generally considered to be equivalent to monotonic

fracture. Hence, the maximum stress intensity value during the cycle when the fatigue crack propagation becomes unstable should correlate with the monotonic fracture toughness,

$$K_{\max}\left(\Delta K_{\mathrm{I}}^{\max}\right) \equiv \frac{\Delta K_{\mathrm{I}}^{\max}}{1-R} = K_{\mathrm{IC}}. \quad (6)$$

In Fig. 8, $\Delta K_{\mathrm{I}}^{\max}$ values from Table 3 are plotted against the corresponding K_{IC} values from Table 2 for the range of microcapsule sizes and concentrations tested. With the exception of neat epoxy, the data for microcapsule filled epoxy falls close to a line with a slope less than unity ($K_{\mathrm{IC}} > K_{\max}(\Delta K_{\mathrm{I}}^{\max})$), indicating a trend of increasing fatigue crack growth resistance with increasing monotonic fracture toughness. A similar trend has been reported previously for rubber-modified epoxies [5, 8, 9, 13], implying that the failure mechanisms for static fracture and fatigue failure in modified epoxies are comparable.

For neat epoxy the $K_{\max}(\Delta K_{\mathrm{I}}^{\max})$ value at fatigue crack instability exceeds the static fracture toughness values K_{IC}. This anomalous behavior has been reported previously for other filled polymer systems [5, 11, 12, 14]. The inconsistency between $K_{\max}(\Delta K_{\mathrm{I}}^{\max})$ and K_{IC} is explained by differences in the crack-tip geometry [33] and to a lesser degree the loading rate [5, 34] between monotonic and fatigue testing. Montonic fracture toughness values are determined using precracks generated by a razor blade as prescribed in ASTM Standard D 5045. In contrast, the maximum stress intensity values $K_{\max}$ are determined for a crack tip generated in fatigue by progressively increasing ΔK_{I}. As described by Xiao et al. [33], yielding and damage at the crack tip under cyclic loading can cause

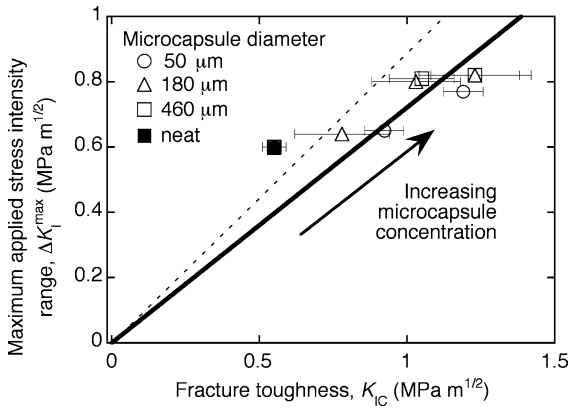

Fig. 8 Influence of K_{IC} on $\Delta K_{\mathrm{I}}^{\max}$. The dashed line corresponds to the maximum applied stress intensity range $\Delta K_{\mathrm{I}}^{\max}$ for fatigue crack instability when $K_{\max}(\Delta K_{\mathrm{I}}^{\max}) \equiv \Delta K_{\mathrm{I}}^{\max}/(1-R) = K_{\mathrm{IC}}$. The solid line is the best linear fit through the data points and the origin

apparent fracture toughness values for DGEBA epoxy with precracks generated by fatigue to exceed fracture toughness values measured in samples with razor blade generated precracks by as much as 31%. Hence, the high value of $\Delta K_{\mathrm{I}}^{\max}$ for neat epoxy is an artifact of the specimen loading history introducing progressive blunting at the crack tip. This effect was only observed in the neat epoxy and is not present in the microcapsule modified systems.

In addition to the toughening mechanisms induced by the embedded microcapsules, the flow of fluid released into the crack plane provides a crack tip shielding mechanism that can improve resistance to fatigue crack propagation. Several authors have reported that hydrodynamic pressure due to viscous flow within a fatigue crack reduces the effective range of Mode-I stress intensity and hence the fatigue crack growth rate for metal submerged in oil [35–38]. During cyclic loading, the crack volume changes significantly with time, requiring fluid flow into and out of the crack. When the crack contains a viscous fluid, the forces required to squeeze the fluid out of the crack during unloading and draw fluid into the crack during loading can be sufficient to shield the crack tip. Reduced crack growth rates in epoxy due to crack tip shielding from viscous fluid flow have been demonstrated for infiltration of both precatalyzed dicyclopentadiene and mineral oil [20].

Conclusions

Fatigue crack propagation was investigated in epoxy toughened with liquid-filled urea-formaldehyde (UF) microcapsules. The addition of microcapsules significantly decreased the fatigue crack growth rate and increased the fatigue life above a transition value of the stress intensity factor ΔK_{T}. Below ΔK_{T} the fatigue behavior was unaffected by the embedded microcapsules. The transition value between these two regimes corresponded to loading conditions where the size of the plastic zone approached the size of the embedded microcapsules. The fatigue-crack growth rate dependence on applied range of stress intensity ΔK_{I} was accurately captured by the Paris power law in both neat epoxy and epoxy with embedded microcapsules. The Paris law exponent n was strongly dependent on the microcapsule concentration, varying from 9.7 for neat epoxy to approximately 4.5 above 10 wt% microcapsules, but was independent of microcapsule diameter. The onset of unstable fatigue-crack growth $\Delta K_{\mathrm{I}}^{\max}$ increased with monotonic fracture toughness, and was independent of microcapsule diameter.

Improved resistance to fatigue crack propagation, was attributed to toughening mechanisms induced by the embedded microcapsules as evidenced by changes in the fatigue fracture plane morphology. In addition to increasing the inherent fatigue life of epoxy, embedded microcapsules filled with an appropriate healing agent offer a potential mechanism to further extend fatigue life through self-healing of fatigue damage.

Acknowledgments The authors gratefully acknowledge support from the AFOSR Aerospace and Materials Science Directorate Mechanics and Materials Program (Award No. F49620-00-1-0094), the National Science Foundation (NSF CMS0218863), and Motorola Labs, Motorola Advanced Technology Center, Schaumburg Ill. Any opinions, findings, and conclusions or recommendations expressed in this publication are those of the authors and do not necessarily reflect the views of the AFOSR or Motorola Labs. The authors would also like to thank Profs. J.S. Moore and P.H. Geubelle of the Autonomic Materials Laboratory of the Beckman Institute of Advanced Science and Technology and Dr. A. Skipor of Motorola Labs for technical support and helpful discussions. Electron microscopy was performed in the Imaging Technology Group, Beckman Institute, of the University of Illinois at Urbana-Champaign, with the assistance of S. Robinson. LAUR-04-2668.

References

1. Cardoso RJ, Shukla A, Bose A (2002) J Mater Sci 37:603
2. Bagheri R, Pearson RA (1996) J Mater Sci 31:4529
3. Skibo MD, Hertzberg RW, Manson JA, Kim SL (1977) J Mater Sci 12:531
4. Paris PC, Gomez MP, Anderson WE (1961) The Trend in Engineering at the University of Washington 13:9
5. Karger-Kocsis J, Friedrich K (1993) Compos Sci Technol 48:263
6. Nagasawa M, Kinuhata H, Koizuka H, Miyamoto K, Tanaka T, Kishimoto H, Koike T (1995) J Mater Sci 30:1266
7. McMurray MK, Amagi S (1999) J Mater Sci 34:5927
8. Becu L, Maazouz A, Sautereau H, Gerard JF (1997) J Appl Polym Sci 65:2419
9. Rey L, Poisson N, Maazouz A, Sautereau H (1999) J Mater Sci 34:1775
10. Hayes BS, Seferis JC (2001) Polym Compos 22:451
11. Azimi HR, Pearson RA, Hertzberg RW (1996) Polym Eng Sci 36:2352
12. Azimi HR, Pearson RA, Hertzberg RW (1995) J Appl Polym Sci 58:449
13. Sautereau H, Maazouz A, Gerard JF, Trotignon JP (1995) J Mater Sci 30:1715
14. Azimi HR, Pearson RA, Hertzberg RW (1996) J Mater Sci 31:3777
15. Brown EN, White SR, Sottos NR (2004) J Mater Sci 39:1703
16. White SR, Sottos NR, Geubelle PH, Moore JS, Kessler MR, Sriram SR, Brown EN, Viswanathan S (2001) Nature 409:794
17. Brown EN, Sottos NR, White SR (2002) Exp Mech 42:372
18. Kessler MR, Sottos NR, White SR (2003) Composites Part A 34:743
19. Brown EN, Kessler MR, Sottos NR, White SR (2003) J Microencapsul 20:719
20. Brown EN (2003) In: Fracture and Fatigue of a self-healing polymer composite material, PhD dissertation, University of Illinois at Urbana-Champaign
21. Rzeszutko AA, Brown EN, Sottos NR (2004) 2003 Proceedings of 5th Undergraduate Research Conf. in Mechanics, University of Illinois at Urbana-Champaign, TAM Report No. 1041, 27
22. Mostovoy S, Crosley PB, Ripling EJ (1967) J Mater 2:661
23. Wang WZ, Li CT, Ye FX (2004) Vacuum 73:649
24. Blackman BRK, Hadavinia H, Kinloch AJ, Paraschi M, Williams JG (2003) Engng Fract Mech 70:233
25. Macon DJ, Anderson GL (2002) J Appl Polym Sci 86:1821
26. Beres W, Koul AK, Thambraj R (1997) J Test Eval 25:2419
27. Cammino R, Gosz M, Mostovoy S (2000) In: Proceedings of ASME International Congress and Exposition 415:17
28. Kessler MR (2002) In: Characterization and performance of a self-healing composite material, PhD dissertation, University of Illinois at Urbana-Champaign
29. Saxena A, Hudak SJ Jr (1978) Int J Fract 14:453
30. Karger-Kocsis J, Friedrich K (1992) Colloid Polym Sci 270:549
31. Chudnovsky A, Kim A, Bosnyak CP (1992) Int J Fract 55:209
32. Irwin GR (1960) Proceedings of 7th Sagamore Ornance Mater. Res. Conf. 4:63
33. Xiao K, Ye L, Kwok YS (1998) J Mater Sci 33:2831
34. Araki W, Adachi T, Gamou M, Yamaji A (2002) Proc I Mech E Part L 216:79
35. Endo K, Okada T, Komai K, Kiyota M (1972) Bull Japan Soc Mech Eng 15:1316
36. Galvin G, Naylor H (1964) Proc Inst Mech Eng J 179:56
37. Plumbridge WJ, Ross PJ, Parry JSC (1985) Mater Sci Eng 68:219
38. Polk C, Murphy W, Rowe C (1975) ASLE Transactions 18:290